inant contribution from $>10^6$-g objects. At the same time, it suggests that the significant mass flux from such bodies predicted on the basis of the Spacewatch results is not well represented in the geochemical data, possibly because it is distributed only locally.

In closing, we would like to note that the current extraterrestrial mass flux measurement could be improved by the use of detectors with larger surfaces or exposure times. Any experiments should, however, be carried out soon, as the projected increase in the flux of artificial orbital debris may seriously compromise the sensitivity of similar measurements in the future (*33*).

REFERENCES AND NOTES

1. E. Grün, H. A. Zook, H. Fechtig, R. H. Giese, *Icarus* **62**, 244 (1985).
2. G. J. Flynn and D. S. McKay, *J. Geophys. Res.* **95**, 14497 (1990).
3. W. H. Ip, *Nature* **345**, 511 (1990).
4. E. Anders, *ibid.* **342**, 255 (1989).
5. C. F. Chyba, P. J. Thomas, L. Brookshaw, C. Sagan, *Science* **249**, 366 (1990).
6. C. Chyba and C. Sagan, *Nature* **355**, 125 (1992).
7. B. K. Esser and K. K. Turekian, *Geochim. Cosmochim. Acta* **52**, 1383 (1988).
8. R. Ganapathy, *Science* **220**, 1158 (1983).
9. F. T. Kyte and J. T. Wasson, *ibid.* **232**, 1225 (1986).
10. M. Takayanagi and M. Ozima, *J. Geophys. Res.* **92**, E641 (1987); D. L. Anderson, *Science* **261**, 170 (1993).
11. D. W. Hughes, in *Cosmic Dust*, J. A. M. McDonnell, Ed. (Wiley, Chichester, United Kingdom, 1978), pp. 123–185.
12. G. W. Wetherill and E. M. Shoemaker, *Geol. Soc. Am. Spec. Pap.* **190**, 1 (1982).
13. D. L. Rabinowitz, *Astrophys. J.* **407**, 412 (1993); but see also D. L. Rabinowitz *et al.*, *Nature* **363**, 704 (1993) for discussion of possible origins of these objects.
14. Z. Ceplecha, *Astron. Astrophys.* **263**, 361 (1992).
15. R. J. Naumann, "The Near-Earth Meteoroid Environment," *NASA TN D-3717* (National Aeronautics and Space Administration, Washington, DC, 1966).
16. T. H. See *et al.*, in "LDEF—69 Months in Space," *NASA CP-3134*, A. S. Levine, Ed. (National Aeronautics and Space Administration, Washington, DC, 1991), pp. 477–486.
17. T. See, M. Allbrooks, D. Atkinson, C. Simon, M. Zolensky, *Meteoroid and Debris Impact Features Documented on the Long Duration Exposure Facility: A Preliminary Report* (Lyndon B. Johnson Space Center, Houston, TX, 1990).
18. M. R. Laurance and D. E. Brownlee, *Nature* **323**, 136 (1986).
19. J. A. M. McDonnell, S. P. Deshpande, D. H. Niblett, M. J. Neish, P. J. Newman, in *Proceedings of IAF/COSPAR World Congress*, W. Flury, Ed. (Pergamon, Oxford, in press).
20. B. G. Cour-Palais, *Int. J. Impact Eng.* **5**, 221 (1987).
21. E. L. Christiansen, *AIAA Pap. #92-1462* (1992).
22. J. A. M. McDonnell and K. Sullivan, in *Proceedings of Workshop on Hypervelocity Impacts in Space*, J. A. M. McDonnell, Ed. (Unit for Space Sciences, University of Kent, Canterbury, United Kingdom, 1992), pp. 39–47.
23. F. Hörz *et al.*, in (*16*), pp. 487–501.
24. S. G. Love, D. J. Joswiak, D. E. Brownlee, in *Lunar Planet. Sci.* **XXIV**, 901 (1993).
25. J. E. Erickson, *J. Geophys. Res.* **73**, 3721 (1968).
26. D. J. Kessler, *AIAA J.* **7**, 2337 (1969).
27. H. A. Zook, in (*16*), pp. 569–579.
28. S. G. Love, University of Washington, thesis (1993).
29. J. S. Dohnanyi, in (*11*), pp. 527–605.
30. M. Imamura, T. Inoue, K. Nishiizumi, S. Tanaka, paper OG 12-21 presented at the 16th International Cosmic Ray Conference, Kyoto, Japan, 1979.
31. M. Maurette, C. Jehanno, E. Robin, C. Hammer, *Nature* **328**, 699 (1987).
32. T. J. Kane and C. S. Gardner, *Science* **259**, 1297 (1993).
33. D. J. Kessler and B. G. Cour-Palais, *J. Geophys. Res.* **83**, 2637 (1978).
34. We thank W. M. Berrios and W. H. Kinard for providing access to the unique surfaces used in this experiment and D. H. Humes for advice and for preparation and handling of the panels. We thank the LDEF Meteoroid and Debris Special Investigation Group for obtaining and archiving the crater images on panels H13, H19, and H25, especially T. H. See for extracting and transmitting the appropriate data. We also thank F. Hörz and H. A. Zook for useful advice and discussions, N. L. King for carrying out the small crater scan, and C. F. Chyba and an unidentified referee for valuable comments and suggestions on this paper. This work was supported by the National Aeronautics and Space Administration.

19 April 1993; accepted 20 August 1993

Melting of (Mg,Fe)SiO_3-Perovskite to 625 Kilobars: Indication of a High Melting Temperature in the Lower Mantle

A. Zerr and R. Boehler

The melting curves of two compositions of (Mg,Fe)SiO_3-perovskite, the likely dominant mineral phase in the lower mantle, have been measured in a CO_2 laser–heated diamond cell with direct temperature measurements and in situ detection of melting. At 625 kilobars, the melting temperature is 5000 ± 200 kelvin, independent of composition. Extrapolation to the core-mantle boundary pressure of 1.35 megabar with three different melting relations yields melting temperatures between 7000 and 8500 kelvin. Thus, the temperature at the base of the lower mantle, accepted to lie between 2550 and 2750 kelvin, is only at about one-third of the melting temperature. The large difference between mantle temperature and corresponding melting temperature has several important implications; particularly the temperature sensitivity of the viscosity is reduced thus allowing large lateral temperature variations inferred from seismic tomographic velocity anomalies and systematics found in measured velocity-density functions. Extensive melting of the lower mantle can be ruled out throughout the history of the Earth.

The interpretation and understanding of geochemical differentiation of the Earth, geodynamics, rheology, and, more recently, seismic tomography data hinge upon the melting temperatures of the lower mantle constituents: For example, (i) differentiation strongly depends on the degree of partial melting that occurred early in Earth's history; (ii) viscosity and anelasticity scale with the ratio of actual temperature over melting temperature, T/T_m; and (iii) the melting temperature limits lateral temperature variations and the temperature contrast between the bottom of the mantle and the core. (Mg,Fe)SiO_3-perovskite is most likely the dominant phase in the lower mantle [up to ~20% magnesiowüstite [(Mg,Fe)O] is also likely present]. Because perovskite melts closely to the eutectic in the MgO-SiO_2 system and the iron content of the mantle is only ~10%, the melting temperature of Mg-Fe-Si-perovskite represents a lower bound for the melting temperature of the lower mantle.

Earlier estimates of the melting curve of (Mg,Fe)SiO_3-perovskite show extreme variations, and melting temperatures predicted for pressures equivalent to those at the bottom of the mantle range from less than 2500 to 8000 K. Earlier experimental studies of melting of perovskite in the diamond cell have large uncertainties and are in strong contradiction to each other in both melting temperature and slope of the melting curve (*1*). Thermodynamic estimates rely on poorly known physical data obtained at low pressure and require a melting relation for extrapolation to mantle pressures (*2*). Molecular dynamics calculations do not provide meaningful constraints on the melting curve (*3*). More accurate multianvil data do not extend to pressures greater than 250 kbar (*4*) and yield only a weak constraint on the melting slope of perovskite above the majorite-perovskite-liquid triple point at about 220 kbar.

To reduce these uncertainties, we investigated the melting of Fe-Mg perovskite using a recently developed diamond-cell technique (5) in which thin section samples are embedded in an argon pressure medium and heated with a high-power CO_2 laser. This method circumvents the experimental problems of earlier laser-heating experiments, which caused large systematic errors; particularly, it avoids large temperature gradients and allows direct temperature

---

Max-Planck-Institut fur Chemie, Postfach 3060, 55020 Mainz, Germany.

measurement and direct detection of melting (Fig. 1), which was not possible with earlier methods. Melting was measured by slowly increasing the laser power until convective motion could be observed, which was accompanied by a drastic increase in the absorption of the laser light by the sample. Rounded melting features with clear signs of recrystallization in the sample were observed under the microscope upon temperature quenching (Fig. 2). Texture and crystallinity of samples held just below the melting temperature remained essentially unaltered even after prolonged heating. Raman spectra of the samples quenched from above the melting temperature were weak, but clearly showed the presence of crystalline perovskite and no indication of vitrification to the highest pressures of this work.

We obtained melting data between 220 and 625 kbar (Fig. 3) using natural single crystals of $(Mg_{.88}Fe_{.12})SiO_3$-orthopyroxene from an alpine lherzolite (Ivrea, Italy), synthetic $MgSiO_3$-enstatite, or enstatite glass as starting material. The temperature range of at least five measurements of the onset of melting was typically less than 400 K. The uncertainty in pressure is mainly attributed to the use of a limited number of ruby chips in the pressure cell, a precaution taken to avoid chemical reaction with the sample. The melting curves determined for both compositions are identical within the experimental uncertainty and are in good agreement with multi-anvil data at lower pressure (*4*). The slope above the majorite-perovskite-liquid triple point at about 220 kbar is about 6 K/kbar, decreasing to about 4 K/kbar at 600 kbar. The determined melting curve is at considerably greater temperatures than curves determined from data obtained with YAG-laser heating in a diamond cell without a pressure medium (*1*). The extremely large temperature gradients in those experiments caused large systematic errors in the temperature measurements and in the detection of melting. The good agreement with the calculated melting curve by Ohtani (*2*) may be fortuitous because the numerous thermodynamic parameters that are required to calculate the melting slope above the majorite-perovskite-liquid triple point were poorly constrained at that time.

We extrapolated our melting curve to

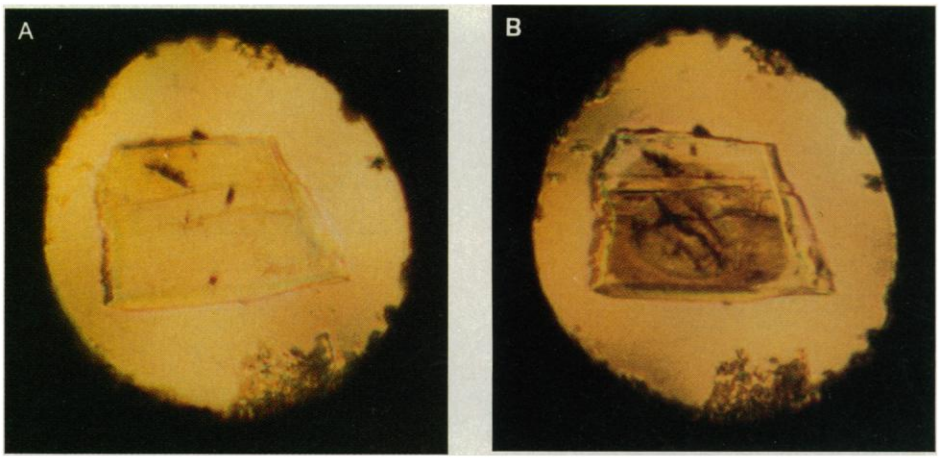

Fig. 2. (**A**) Unheated sample of natural $(Mg_{.88}Fe_{.12})SiO_3$-orthopyroxene at 625 kbar in an argon pressure medium. Sample dimensions are approximately 80 by 50 by 15 μm. (**B**) Sample after melting experiment. The melted portion (round feature), about 30 μm in diameter, shows signs of recrystallization. The larger darkened portion shows the transition to perovskite, as evident from micro-Raman spectra.

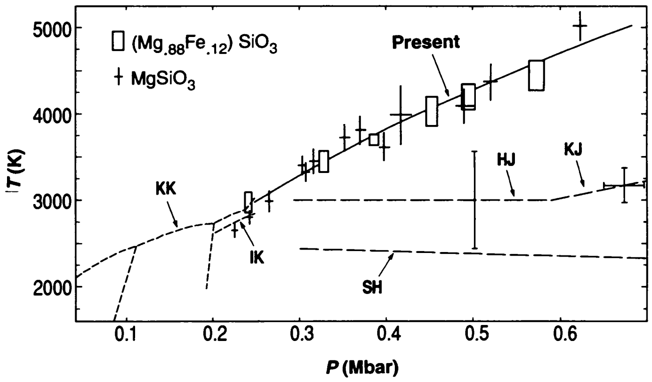

Fig. 3. Experimental results on melting of (Mg,Fe)-SiO_3-perovskite. The present melting curve is a fit to all the data from both compositions and is nearly identical for all three melting relations (*6*). Vertical bars represent the variation of at least five different temperature measurements at the onset of melting at constant pressure. KK and IK curves (*4*) are from multi-anvil experiments (abbreviations refer to authors of studies). SH, HJ, and KJ (*1*) are results of YAG-laser heating experiments on polycrystalline samples with no pressure medium using indirect melting criteria.

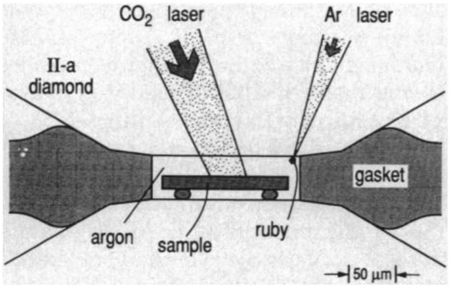

Fig. 1. Schematic cross section through a diamond cell assemblage. A thin sample, thermally insulated from the diamonds by an argon pressure medium, is heated with a broad CO_2-laser beam. This technique produces small axial and radial temperature gradients in the sample (*5*). Temperatures were measured from areas with 3 to 5 μm in diameter.

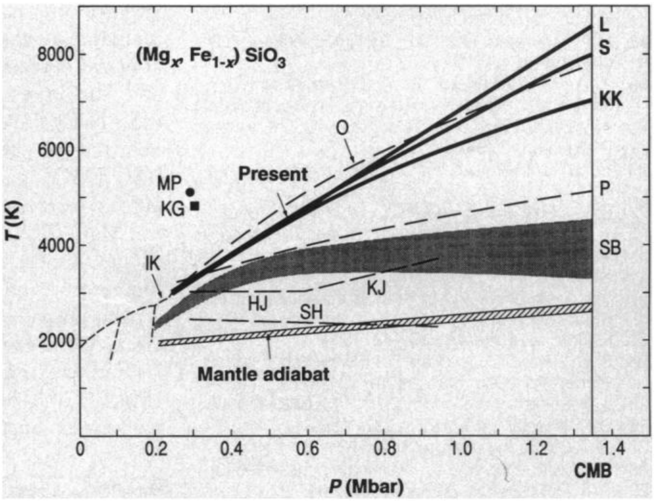

Fig. 4. Melting temperatures of (Mg,Fe)SiO_3-perovskite for the pressure range of the lower mantle. The results of fitting our melting data to the melting relations listed in (*6*) and the extrapolated melting temperatures to the CMB are shown along with all previous estimates from thermodynamic calculations [O, P, and SB (*2*)], molecular dynamics calculations [MP and KG (*3*)], and previous laser-heating experiments [HJ, SH, and KJ (*1*)]. An approximate mantle geotherm, shows the large difference between adiabatic gradient and melting gradient in the lower mantle.

higher pressures by three frequently used melting relations: the two empirical relations by Simon and Kraut-Kennedy and the quasi-theoretical melting criterion by Lindemann (6) (Fig. 4). We estimate that the melting temperature of (Mg,Fe)SiO$_3$-perovskite at the core-mantle boundary (CMB) is between 7000 and 8500 K. This temperature and the melting curve are also significantly higher than well-accepted temperatures of the lower mantle geotherms (Fig. 4).

Most likely, the melting temperature of the lower mantle is not substantially below that of perovskite, because perovskite melts near the eutectic of the Mg-Fe-Si-O system (4), which represents lower mantle chemistry. If this conclusion holds, the extremely large difference between the temperature of the lower mantle and the melting temperature of perovskite has some important geophysical and geochemical implications: (i) Large-scale melting and chemical differentiation of the lower mantle resulting from formation and separation of a melt can be excluded, even if the Earth was significantly hotter in past geologic times. (ii) The temperature dependence of physical properties related to the shear modulus such as viscosity and anelasticity scale with the homologous temperature, T/T_m. The data suggest that the dependence is most reduced in the lower mantle, because this value decreases significantly with depth. (iii) The high melting temperatures of perovskite allow the existence of a large thermal boundary across the D region between mantle and core (7). (iv) Large lateral seismic velocity anomalies in the lower part of the mantle, found from seismic tomography, may result from large variations in temperature (8) because such variations would not necessarily result in partial melting or large decreases in the viscosity.

REFERENCES AND NOTES

1. D. L. Heinz and R. Jeanloz, *J. Geophys. Res.* **92**, 11437 (1987); E. Knittle and R. Jeanloz, *Geophys. Res. Lett.* **16**, 421 (1989); J. S. Sweeney and D. L. Heinz, *ibid.* **20**, 855 (1993). The YAG-laser beam, used in these experiments, had to be tightly focused because of the low optical absorption and the lack of a thermally insulating pressure medium. This produced a complicated three-dimensional temperature distribution with extremely large temperature (and pressure) gradients in the polycrystalline sample, which served as its own pressure medium. This situation did not allow a direct measurement of the temperature in the center of the hot spot and temperatures had to be calculated from the measured average temperatures. Melting was not directly detected; instead isotropic optical behavior subsequent to quenching, and indirect thermal analysis were used as the melting criteria.
2. E. Ohtani, *Phys. Earth Planet. Inter.* **33**, 12 (1983); J. P. Poirier, *ibid.* **54**, 364 (1989); L. Stixrude and M. S. T. Bukowinski, *J. Geophys. Res.* **95**, 19311 (1990).
3. M. Matsui and G. D. Price, *Nature* **351**, 735 (1991); B. Kapusta and M. Guillope, *Phys. Earth Planet. Inter.* **75**, 205 (1993).
4. E. Ito and T. Katsura, in *High-Pressure Research: Application to Earth and Planetary Sciences*, Y. Syono and M. H. Manghnani, Eds. (TERRAPUB, Tokyo/American Geophysical Union, Washington, DC, 1992), pp. 315–322; T. Kato and M. Kumazawa, *Nature* **316**, 803 (1985). The maximum pressures in these experiments were 250 and 200 kbar, respectively. Use of thermocouples at these pressures leads to an uncertainty in temperature of at least ±100 K.
5. R. Boehler and A. Chopelas, *Geophys. Res. Lett.* **18**, 1147 (1991); in *High-Pressure Research: Application to Earth and Planetary Sciences*, Y. Syono and M. H. Manghnani, Eds. (TERRAPUB, Tokyo/American Geophysical Union, Washington, 1992), pp. 55–60. The three essential features of this laser-heating technique are CO$_2$-laser radiation, an argon pressure medium, and thin section samples. The high power of CO$_2$-lasers, the high absorption of its radiation by minerals, the low thermal conductivity of argon, and the small sample thickness, reduce both radial and axial temperature gradients. Temperatures were measured in situ from the center of the hot spot from areas with 3 to 5 μm in diameter, using a Planck radiation function and solving for both temperature and emissivity, assuming wavelength-independent emissivities. This assumption is probably reasonable for transparent minerals in the spectral range of 530 to 830 nm used in the present measurements. Corrections similar to the known emissivity-wavelength-temperature functions for metals would decrease temperatures by about 100 K at 3000 K and 350 K at 5000 K. Other uncertainties in the temperature measurements, associated with radial or axial temperature gradients, optical geometry, chromatic abberation, and curve fitting add up to less than 100 K in this experiment. The method does not require any correction of the directly measured temperature. Pressures were measured from ruby chips, distributed throughout the pressure cell. Thermal pressures in the melting experiments were small because of the small volume ratios between sample and the argon pressure medium.
6. The Simon equation [F. Simon and G. Glatzel, *Z. Anorg. Allg. Chem.* **178**, 309 (1929)] is a power-law relationship between pressure and melting temperature that describes the low-pressure melting behavior of a number of substances reasonably well. The Kraut-Kennedy relation is an empirical linear dependence of the melting temperature, T_m, and the volume, based on observations made on the highly compressible alkali metals [E. A. Kraut and G. C. Kennedy, *Phys. Rev. Lett.* **16**, 608 (1966)]. It has been recently found to describe well the melting behavior of a number of metals and oxides to high compression [R. Boehler, *Earth Planet. Sci. Lett.* **111**, 217 (1992)]. The Lindemann relation [F. A. Lindemann, *Phys. Z.* **11**, 609 (1910)] states that melting occurs when the vibrational amplitude of the atoms (or molecules) reaches a critical fraction of the interatomic distance. This melting relation was used in the form $d\ln T_m/d\ln\rho = 2(\gamma - 1/3)$, where ρ is the density, and γ is the Gruneisen parameter. The pressure dependence of γ was taken from systematics found in direct measurements of the Grüneisen parameter of a large number of materials by R. Boehler and J. Ramakrishnan [*J. Geophys. Res.* **85**, 6996 (1980)], as $d\ln\gamma/d\ln\rho = 1.3 \pm 0.3$.
7. R. Boehler [*Nature* **363**, 534 (1993)] estimated a minimum temperature increase across the core-mantle boundary of 1300 K from static melting experiments of iron and iron-oxygen compounds to 2 Mbar.
8. D. A. Yuen, O. Cadek, A. Chopelas, and C. Matyska [*Geophys. Res. Lett.* **20**, 899 (1993)] calculated lateral temperature variations, δT, from the measured seismic anomalies, $\delta v/v$ [W.-J. Su and A. M. Dziewonski, *Phys. Earth Planet. Inter.* **74**, 29 (1992)], and new measurements of sound velocities of several minerals at mantle pressures, and pressure systematics of the thermal expansion coefficient, α, using $\delta T = (\delta v/v)(d\ln\rho/d\ln v)/\alpha$. Their values of δT are still uncertain, but show a trend toward high-temperature anomalies in excess of 1000 K.

9. We thank A. Chopelas and D. Yuen for helpful discussions and A. Chopelas for constructive comments on the manuscript.

6 July 1993; accepted 1 September 1993

3.4-Billion-Year-Old Biogenic Pyrites from Barberton, South Africa: Sulfur Isotope Evidence

Hiroshi Ohmoto,* Takeshi Kakegawa, Donald R. Lowe

Laser ablation mass spectroscopy analyses of sulfur isotopic compositions of microscopic-sized grains of pyrite that formed about 3.4 billion years ago in the Barberton Greenstone Belt, South Africa, show that the pyrite formed by bacterial reduction of seawater sulfate. These data imply that by about 3.4 billion years ago sulfate-reducing bacteria had become active, the oceans were rich in sulfate, and the atmosphere contained appreciable amounts (>>10^{-13} of the present atmospheric level) of free oxygen.

Sulfate is the second most abundant anion in present-day seawater. It is generated primarily on land by weathering of SO$_4^{2-}$ minerals and pyrite (FeS$_2$) under an O$_2$-bearing atmosphere and is transported by rivers to the oceans where it is converted to SO$_4^{2-}$ minerals, chiefly by evaporation of seawater, and to pyrite. The pyrite forms mostly in normal marine sediments where SO$_4^{2-}$ supplied from the overlying seawater is converted to H$_2$S (that is, reduction of S^{6+} to S^{2-}) by SO$_4^{2-}$-reducing bacteria (SRB); the H$_2$S reacts with Fe-bearing minerals in the sediments to form pyrite. After burial, lithification, metamorphism, and uplift, exposure of marine sedimentary rocks to air generates SO$_4^{2-}$. The present-day cycles of sulfur in the Earth, therefore, are controlled by the presence of free O$_2$ in

---

H. Ohmoto and T. Kakegawa, Department of Geosciences, The Pennsylvania State University, University Park, PA 16802, and Institute of Mineralogy, Petrology, and Economic Geology, Tohoku University, Sendai 980, Japan.
D. R. Lowe, Department of Geology, Stanford University, Stanford, CA 94305.